coatings

MDPI

Article

Easy and Fast Fabrication of Self-Cleaning and Anti-Icing Perfluoroalkyl Silane Film on Aluminium

Peter Rodič [1,*], Barbara Kapun [1], Matjaž Panjan [2] and Ingrid Milošev [1]

[1] Jožef Stefan Institute, Department of Physical and Organic Chemistry, Jamova c. 39, SI-1000 Ljubljana, Slovenia; barbara.kapun@ijs.si (B.K.); ingrid.milosev@ijs.si (I.M.)
[2] Jožef Stefan Institute, Department of Thin Films and Surfaces, Jamova c. 39, SI-1000 Ljubljana, Slovenia; matjaz.panjan@ijs.si
* Correspondence: peter.rodic@ijs.si; Tel.: +386-1-4773-261

Received: 12 February 2020; Accepted: 28 February 2020; Published: 4 March 2020

Abstract: A combination of the chemical etching process in $FeCl_3$ solution and chemical surface grafting by immersion in ethanol solution containing 1H,1H,2H,2H-perfluorodecyltriethoxysilane is a viable route to achieve a hierarchical surface topography and chemical bonding of silane molecules on an aluminium surface leading to (super)hydrophobic characteristics. Characterisation of untreated and treated aluminium surfaces was carried out using contact profilometry, optical tensiometry, scanning electron microscopy coupled with energy-dispersive spectroscopy and X-ray photoelectron spectroscopy to define the surface topography, wettability, morphology and surface composition. Additionally, the dynamic characteristics were evaluated to define bouncing and the self-cleaning effect. A thermal infrared camera was employed to evaluate anti-icing properties. The micro/nano-structured etched aluminium surface grafted with perfluoroalkyl silane film showed excellent superhydrophobicity and bounce dynamics in water droplet tests. The superhydrophobic aluminium surface exhibited the efficient self-cleaning ability of solid pollutants as well as improved anti-icing performance with melting delay.

Keywords: superhydrophobic surface; bounce dynamics; self-cleaning; anti-icing

1. Introduction

High specific strength, low specific weight and good corrosion resistance at atmospheric conditions are some of the main reasons for the extensive use of aluminium in building construction, transportation industries and many other applications in everyday life [1]. In recent years, rapid developments have been made in the area of superhydrophobic anticorrosive coatings. These coating can act as corrosion protection but offer additional functional abilities of an aluminium surface once exposed to the real environment including adsorption of the pollutants and ice formation [2,3]. The definition of superhydrophobicity is based on the water contact angle of the droplet on the surface which must be larger than 150° and have a sliding angle smaller than 10° [4,5]. Thus, naturally hydrophilic aluminium surfaces should be treated to reduce their wettability. Although in recent years, numerous studies related to superhydrophobic surfaces have reported on their excellent performance [2,3,6], there is still a need to develop a convenient, environmentally acceptable and facile method for fabrication of superhydrophobic aluminium surfaces. The latter can trap air in the modified surface topography which prevents aggressive ions from reaching the aluminium surface, consequently offering an efficient mechanism for corrosion protection [2,3,6–9]. Superhydrophobic surfaces have many applications because of their excellent properties such as on anti-icing [8,10–12], anti-fouling [13] and anti-bacterial properties [14]; therefore, there is a high potential for applications in different fields [3].

The wettability of a solid surface is a function of two primary factors: surface roughness and surface chemistry [5]. There are several routes to construct superhydrophobic surfaces such as a sol-gel process [15], anodic oxidation [16,17], chemical vapour deposition [18] and chemical etching [9,19,20]. However, once the practical application of such a coating is considered, a method with simple operation, low-cost and short operation time are required. From this point of view, chemical etching to produce a roughened surface followed by grafting a low-surface energy organic material, such as fatty acid [9,19] or alkyl and perfluoroalkyl silanes [8], are one of the easiest, economical and environmentally acceptable routes [2,20].

Chemical etching of aluminium has been reported in several studies (e.g., [21]); usually, it is performed in strong acid solutions (e.g., HCl, H_2SO_4) in combination with other reagents such as HCl/H_2O_2 [22], HCl/HF-Beck's solution [23–25] or alkaline solutions (e.g., NaOH) [9,26]. The surface etching process can be performed also in solutions of metal chlorides such as NaCl [25], $CuCl_2$ [27,28], and $FeCl_3$ [21,27,29,30]. A comparative study of various etchants confirms that the best performance was obtained with $FeCl_3$ [27]. The latter is also traditionally known as a home or industrially used circuit board etchant and, thus, a multipurpose chemical compound. The process is safe and environmentally acceptable because the ferric ions themselves are not hazardous. The etching process in $FeCl_3$ is usually performed in combination with the electrochemical process [30], and the optimization and novelty of the process would include the fabrication in the absence of electricity [21]. This kind of etching procedure has hitherto been much less investigated, offering room for improvement.

The grafting of aluminium surfaces with various alkyl and fluoroalkyl silanes [8,29] has been often used in the past due to the low surface energy of the CH, CF_2, CF_3 groups in the chain [8,31]. For instance, the treatment of aluminium or its alloys with fluoroalkyl silanes (FAS) in NaOH solution has been utilized to prepare the superhydrophobic coating [8,25,32–34]. The initial silane precursors were hydrolysed, condensed and covalently bonded on activated aluminium surface forming Al–O–Si bonds in an exothermic process [35,36].

Superhydrophobic properties are the basis for several surface functionalities. In that context, the dynamic characterisation of the water droplet on the surface [32] is essential to understand the self-cleaning [22,37] and anti-icing properties [8–12].

In this current work, (super)hydrophobic films on aluminium surfaces were fabricated using a two-step process consisting of an etching procedure in $FeCl_3$ solution (in the absence of electricity) to form a hierarchical micro/nano-structure aluminium surface and grafting at ambient temperature directly in an ethanol solution of 1H,1H,2H,2H-perfluorodecyltriethoxysilane as a low surface energy material. The surface morphology and composition were studied to explore the correlations between the etching process and grafting. Additionally, the bounce dynamics was studied on the superhydrophobic film to better understand the functional properties such as the self-cleaning ability for solid pollutants and melting delay. The latter was evaluated with an innovative approach using a thermal infrared camera.

2. Materials and Methods

2.1. Metal Substrates and Chemicals

A 1 mm thick aluminium (Al > 99.0%) sheet was distributed by GoodFellow, Cambridge Ltd. (Huntingdon, England). It was cut into 20 mm × 20 mm plates. The surface was sequentially ground with Struers LaboSystem LaboPol-20 machine using 1000, 2000 and 4200 SiC abrasive papers (supplied by Struers ApS, Ballerup, Denmark) in the presence of tap water.

A two-step procedure for producing superhydrophobic aluminium surface included etching in a $FeCl_3$ solution for various durations (5, 10, 15, 20, 25 and 30 min) followed by grafting by immersion in an ethanol solution of perfluoroalkyl silane for 30 min. Etching solution was prepared from iron(III) chloride ($FeCl_3 \times 6H_2O$; powder > 97%, CAS no. 10025-77-1, distributed by Sigma–Aldrich) and Milli-Q Direct water with a resistivity of 18.2 MΩ cm at 25 °C (Millipore, Billerica, MA, USA) in a

volumetric flask to give a concentration of 1 mol/L. Grafting was performed for 30 min in 1 wt.% 1H,1H,2H,2H-perfluorodecyltriethoxysilane – FAS-10 ($C_{16}H_{19}F_{17}O_3Si$, > 97%, CAS no. 101947-16-4, distributed by Sigma–Aldrich) ethanol solution (C_2H_5OH, absolute, anhydrous > 99.9%, CAS no. 64-17-5, distributed by Sigma–Aldrich).

The samples were positioned at the bottom of the beaker with the ground surface facing up. Both steps were performed at room temperature. After each preparation step (i.e., grinding, etching, grafting), the samples were thoroughly rinsed with distilled water and cleaned by immersion in pure ethanol in an ultrasonic bath to remove all grinding/etching residuals, unreacted FAS-10 and other organic substances present on the surface. Finally, the samples were dried with a stream of compressed nitrogen.

2.2. Surface Characterisation

2.2.1. Weight Loss Test

The weight loss test was performed to evaluate the capability of the etching process. Weight loss (given in %) was determined as a difference in weight of a clean and dried aluminium before and after the etching process using a digital precision laboratory analytical weighing scale (Mettler Toledo AE200 Analytical Balance) with a precision of 0.1 mg. The evaluation was performed on five parallel samples. The data are given as average values ± standard deviations. The obtained data were fitted using linear regression to evaluate etching rate, determined by the slope of the curve.

2.2.2. Surface Topography

Surface 3D topography and linear profiles of the etched aluminium after various etching times were evaluated on three randomly chosen spots, employing a stylus contact profilometer, model Bruker DektakXT, using a 2 μm tip and in a soft-touch mode with force 1 mN. The measured surface was 1 mm × 1 mm, the vertical analysis range 65.5 μm and the vertical resolution 0.167 μm/point. Measured data were analysed using TalyMap Gold 6.2 software. Results are presented as 3D images and line profiles, and their corresponding surface roughness (S_a) are given as average values ± standard deviations.

2.2.3. Wettability

Water, diiodomethane and hexane contact angle measurements were performed at room temperature by the static sessile-drop method on a Krüss FM40 EasyDrop contact-angle measuring system. A small liquid droplet (4 μL) was formed on the end of the syringe which was carefully deposited onto the treated aluminium surface. Digital images of the droplet silhouette were captured with a high-resolution camera, and the contact angle was determined by numerically fitting the droplet image using associated protocol software for drop shape analysis. The values reported herein present the average of at least five measurements on various randomly chosen areas and are reported as average values ± standard deviations.

2.2.4. SEM/EDS Characterisation

A field-emission scanning electron microscope (FE-SEM, JEOL JSM 7600 F, Tokyo, Japan) equipped with an energy-dispersive X-ray spectrometer (EDS, Inca 400, Oxford Instruments, Bucks, England) was used to analyse the morphology and composition of aluminium etched in $FeCl_3$ and grafted with FAS-10. Prior to analysis, samples were coated with a few nanometres thick layer of carbon. The FE-SEM imaging was performed using secondary electron detector (SEI mode), lower secondary electron detector (LEI mode) and backscattering electrons for composition (COMPO mode) of the specimens at 5 and 10 kV energy. The EDS analyses were performed at 10 kV in a point analysis mode. The data were normalised and given as an atomic percentage (at.%). The amount of carbon was excluded from the quantitative analysis.

2.2.5. XPS Characterisation

The chemical compositions of the etched aluminium surface and grafted with FAS-10 were analysed with X-ray photoelectron spectroscopy (XPS) using an PHI TFA XPS spectrometer (Physical Electronics, USA) equipped with aluminium and magnesium monochromatized radiation. The XPS survey and high-energy resolution spectra were collected using Al-K_α radiation (1486.92 eV). The pressure in the chamber was in the range of 10^{-9} mbar. A constant analyser energy mode with 187.9 eV pass energy was used for survey spectra and 39.35 eV pass energy for high-energy resolution spectra. Photoelectrons were collected at a take-off angle 45° relative to the sample surface. The positions of all peaks were normalized with respect to C 1s peak at 284.8 eV. The elemental composition given as an atomic percentage (at.%) was determined from the survey XPS spectra using PHI MultiPak V8.0 software.

2.2.6. Bounce Dynamics

The bounce dynamics of a water droplet were investigated with an ultra-high-speed camera Photron FASTCAM SA-Z (Tokyo, Japan), 2000 frames per second, using 105 mm Nikon F2.8G objective (New York, NY, USA) at ambient temperature. A water droplet (10 μL) was formed on the end of the syringe and released onto the specimen surface from 45 mm height. The bouncing of a water droplet upon the horizontal specimen surface (tilted for 2 degrees) was recorded, and the frames of the movie were analysed in order to evaluate the dynamic properties.

2.2.7. Self-Cleaning Ability

The self-cleaning testing was carried out on ground and treated aluminium samples in size of 50 mm × 40 mm by the following procedures: the aluminium sample on a horizontal stage (tilted for 2 degrees). The solid pollution was simulated by covering the aluminium surface with a layer of graphite multiwalled nanotubes (carbon > 95%, length 1–10 μm, PlasmaChem GmbH, Berlin, Germany). Then, a water droplet of 10 μL was dropped onto the surface from a 2 cm height. The flow of solid pollution along with the water droplet was recorded using a digital camera to evaluate the pollutant removal after the water droplet rolled off from the surface.

2.2.8. Anti-Icing Ability

The anti-icing properties were studied on the ground and treated aluminium samples of a 50 mm × 40 mm size under the overcooled conditions. The test was performed with water droplets of 60 μL which were gently placed on the horizontal substrate. The samples were put in the freezer (−15 °C) for 1 h, then taken out and left at room temperature. Meanwhile, the melting process was evaluated by recording the melting times for droplets on non-treated and treated surfaces using a digital camera and thermal Fluke Ti55FT Infrared Camera (Everett, WA, USA). In parallel, the difference in ice adhesion was also evaluated by tilting the samples vertically (90 degrees) and measuring the time at which the frozen droplets were removed/slid from the surface. Additionally, the anti-icing properties were studied on the ground and treated aluminium under overcooled conditions including the water-dripping test. The test was performed in a freezer at −15 °C. The water droplets of cold water (T = 5 °C) were dropped continuously from a 10 cm height with a dripping rate of ~20 mL/min with the surface tilted at 10°.

3. Results and Discussion

3.1. Surface Characterization

The two-step surface treatment to fabricate the (super)hydrophobic aluminium surface consisted of etching in a $FeCl_3$ solution to obtain the hierarchical micro/nano-structure surface followed by grafting the surface in an ethanol solution of FAS-10 as a low surface energy material. According to the

above description, the predicted reaction mechanism during surface treatment (etching + grafting) is schematically presented in Figure 1.

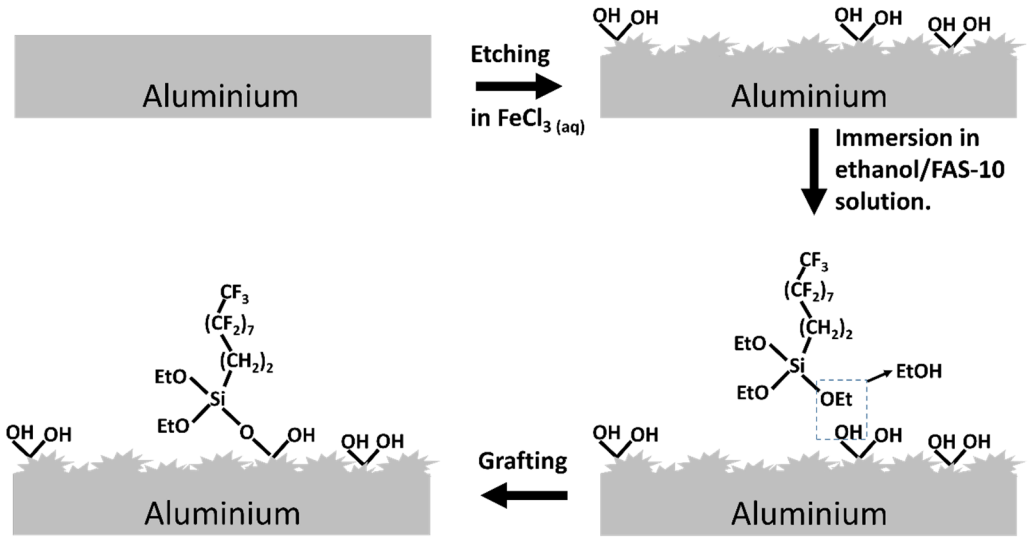

Figure 1. Schematic illustration of the formation of a (super)hydrophobic aluminium surface prepared by the etching process in a $FeCl_3$ solution followed by grafting with perfluoroalkyl silane, FAS-10.

The etching mechanism is based on redox reactions. In the first step, aluminium reacts with ferrous ions in aqueous solution. As a result, aluminium is oxidised and dissolved; at the same time, Fe^{3+} is reduced and transferred into the etchant solution [21,27,38]. The overall oxidation-reduction (redox) reaction of aluminium etching with $FeCl_3$ can be written as follows:

$$Al + Fe^{3+} \rightarrow Al^{3+} + Fe \quad (1)$$

The area of the etched surface is time-dependent and, consequently, also the composition of the aluminium surface due to the progressive removal of the native passive film (Al_2O_3). After taking the aluminium sample from etching solution, it reacts spontaneously with oxygen/humidity during rinsing with water which causes the passivation of the surface due to the formation of fresh aluminium oxide/hydroxide film containing OH^- groups (Figure 1). In the second step, denoted as grafting, there is a reaction between hydroxylated aluminium surface and $(CH_3CH_2O)_3$–Si–$(CH_2)_2(CF_2)_7CF_3$ (FAS), where –OCH_2CH_3 (OEt) presents a hydrolysable ethoxy group and –$(CH_2)_2(CF_2)_7CF_3$, a non-hydrolysable perfluoroalkyl chain, resulting in the formation of surface film (Figure 1). The interfacial condensation and cross-linking reactions take place between the alkoxy and hydroxy groups of the etched aluminium, leading to robust covalent binding between the FAS molecule and the aluminium surface according to Equation (2):

$$\begin{gathered} Al(OH)_3 + (CH_3CH_2O)_3\text{-Si-}(CH_2)_2(CF_2)_7CF_3 \rightarrow \\ Al(OH)_2\text{-O-Si-}(OCH_2CH_3)_2\text{-}(CH_2)_2(CF_2)_7CF_3 + CH_3CH_2OH \end{gathered} \quad (2)$$

The side product of this reaction is ethanol. Such a chemical process is exothermic and, as a result, the monodentate reaction between surface and fluoro-silane is expected [36]. This process allows the integration of $(CH_2)_2(CF_2)_7CF_3$ functional groups on the aluminium surface. The perfluoro groups are oriented outward from the surface due to the long perfluoroalkyl chain [9,39].

To sum up, the presence of Al–OH bonding on the freshly $FeCl_3$-etched aluminium surface is necessary to form a covalent bond between the aluminium surface and silicon, –Si–O–Al [35]. The details on the chemical etching and grafting on the surface are discussed below.

3.1.1. Weight Loss Test

The dissolution of aluminium can be quantitively evaluated using weight loss measurements as a function of immersion time (Figure 2a).

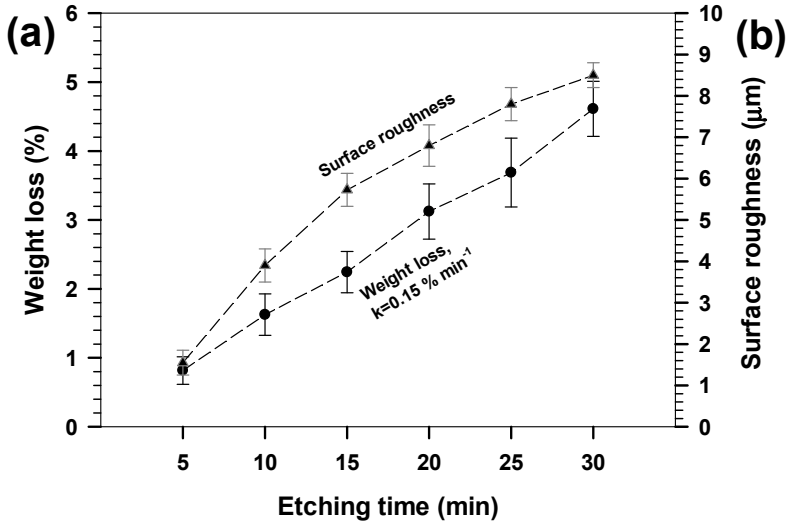

Figure 2. (**a**) Weight loss of aluminium as a function of etching time in 1 M $FeCl_3$ solution, and (**b**) the respective surface roughness determined by contact profilometry. The kinetics of weight loss was estimated from a linear regression of obtained values as a function of etching times.

The intensity of the etching process on the aluminium surface during immersion in $FeCl_3$ solutions could be seen visually due to the aggressive displacement reaction between a freshly ground aluminium surface and Fe ions (seen as bubbles formation and heating the etchant solution). The sample's weight was reduced proportionally with the etching time. At the beginning, the etching was slightly inhibited due to the passive layer of Al_2O_3, which was later (after 5 min) locally removed. The kinetics of the reaction was related to the diffusion process between the substrate and etchant solution. An increase in weight loss after various etching times confirms a high aggressiveness of $FeCl_3$ solution, where every five minutes of etching induced approximately a 0.75% weight loss (the slope of the curve was 0.15% min^{-1} (Figure 2a).

3.1.2. Surface Topography

The surface roughness (S_a) as a function of the etching time by $FeCl_3$ is quantitatively presented in Figure 2b. The ground aluminium had a small surface roughness, S_a = 0.12 ± 0.03. The surface roughness of the 5 min $FeCl_3$-etched aluminium substrate increased by more than 10 fold, to S_a = 1.6 ± 0.3 μm, and continued to increase linearly up to S_a = 5.7 ± 0.4 μm at 15 min. At a longer etching time, the increase in roughness was slower but after 30 min roughness reached S_a = 8.5 ± 0.3 μm. The increase in surface roughness correlated with that of weight loss; therefore, both parameters can be time-controlled.

The 3D surface profiles show that the dimensions of the roughness features were at different scales and that the topography of the surfaces varied significantly with the etching time (Figure 3).

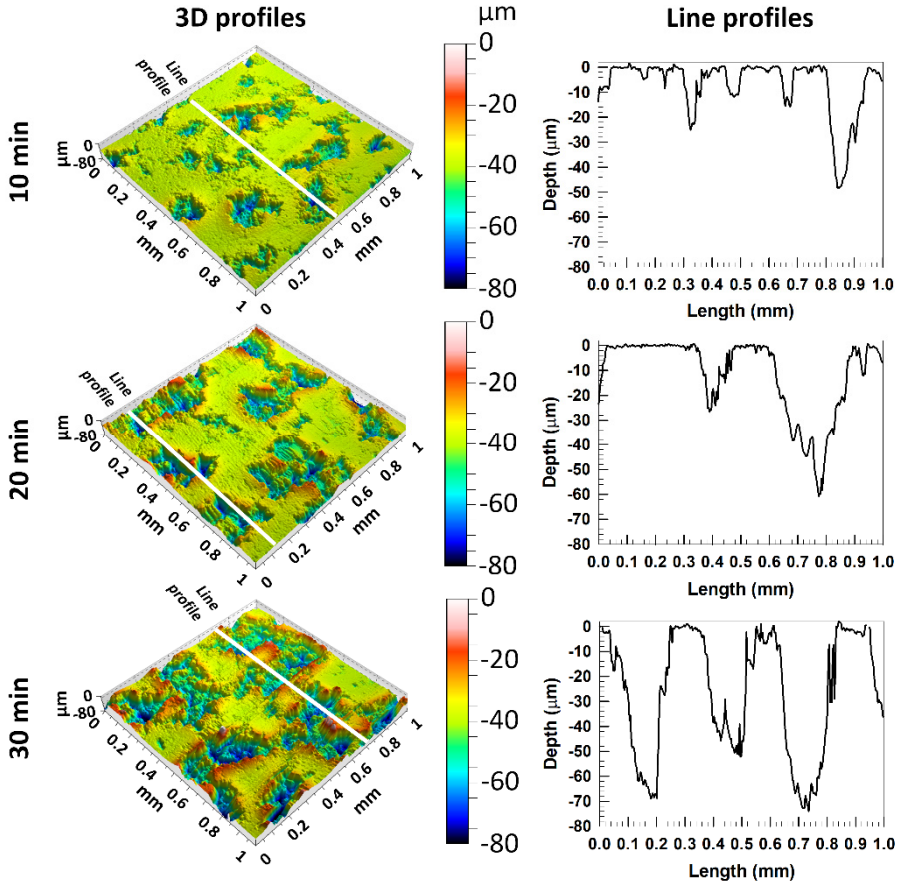

Figure 3. (left panel) 3D surface topography images of aluminium surface etched for 10, 20 and 30 min in 1 M $FeCl_3$ solution. The white lines present the area where single line profiles analyses were performed (right panel). The surface roughnesses determined from 3D profiles are presented in Figure 2.

A macroscale roughness was observed with a variable number of pits. At extended etching times, an increase in the number, size and depth of the pits at the etched aluminium could be observed at both the 3D and line profiles. Moreover, line profiles show that the number of large pits increased three-fold after etching for 30 min compared to that after 10 min; at the same time, their depth almost doubled (from 40 µm to 80 µm). This formation of deep and large pits (Figure 3) explains a slower increase in S_a after longer etching times (Figure 2b).

3.1.3. SEM Characterisation

The topography and morphology of ground and 20 min etched aluminium were characterised using COMPO and LEI modes (Figure 4).

The surface of ground aluminium showed many small pores and some defects that are probably related to the grinding process. Despite the fact that the aluminium used was of 99.0% purity used, it contained impurities that can be seen as bright spots in the SEM image recorded in COMPO mode. The results of the EDS analysis are given in Table 1.

The ground aluminium was mainly composed of Al and O, implying the presence of a thin oxidized layer on the surface (Figure 4a, Table 1, spot 1). It also contained some impurities such as Si and Fe (spots 2, 3). Silicon is related to remnants after the grinding procedure and is seen as dark areas (spot 2), while Fe is an impurity in the metal and forms small Fe-rich intermetallic particles which also contain Si (spot 3).

Table 1. Composition determined by EDS analysis in at.% at enumerated spots on ground and etched aluminium surface using $FeCl_3$ as denoted in Figure 4.

	Numbered Spots	Al	O	Fe	Si
Ground surface	1	40.0	60.0		
	2	39.8	60.0		0.2
	3	29.5	54.6	15.5	0.4
Etched surface	4	82.2	16.5		1.3
	5	98.0	2.0		
	6	56.3	19.9	19.1	4.7

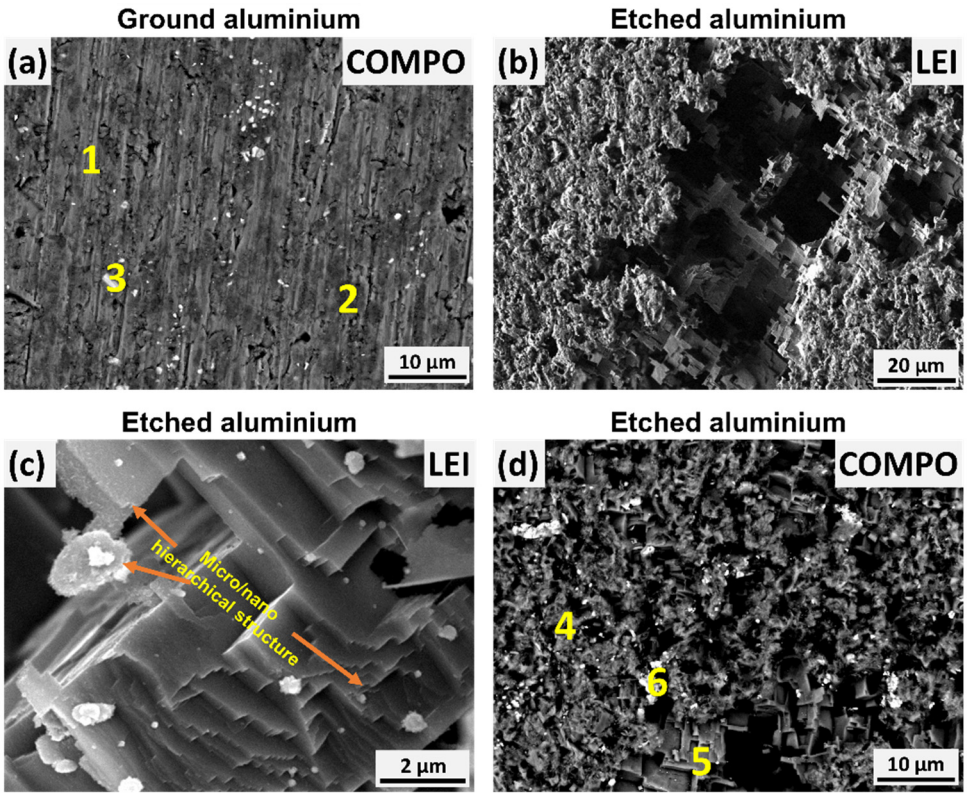

Figure 4. SEM images of (**a**) ground aluminium surface and (**b**–**d**) ground aluminium etched for 20 min in 1 M $FeCl_3$ recorded in COMPO and LEI modes. The enumerated positions (from 1 to 6) indicate spots where the EDS analysis was performed (Table 1).

The SEM LEI image of the surface after etching for 20 min in $FeCl_3$ solution (Figure 4b) shows many small holes and large deep pits. Moreover, the formation of a micro/nano-structured surface pattern compared to the ground surface is evident (Figure 4c,d). Even after etching, the impurities remained at the surface as confirmed by the SEM COMPO image (Figure 4d, Table 1). It is noteworthy that Fe was not present in the aluminium matrix (spots 4,5) which confirms the efficient etching process between Al and Fe without residual Fe on the surface. Iron was detected at spot 6, but the comparison with ground surface (spot 3) indicates that these are Si-containing Fe impurities which were not removed during the etching process.

The morphology of aluminium after various etching times (10, 20 and 30 min) was recorded by SEM using the SEI mode (Figure 5).

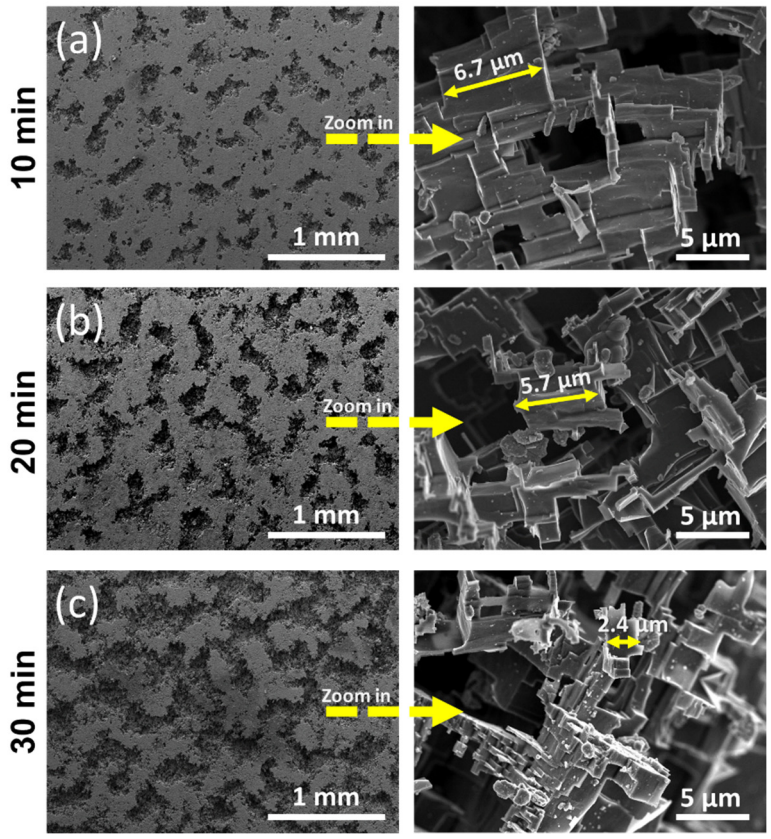

Figure 5. SEM images of surface morphologies of aluminium surface etched for 10, 20 and 30 min in the 1 M $FeCl_3$ solution recorded in SEI mode at lower (left) and higher magnification (right). The arrows present the estimated sizes of the formed hierarchical structures in the formed pits.

Aluminium etched for 10 min shows dispersed rectangular micro-scale pits with a width of about 200 µm distributed throughout the surface (Figure 5a, left). In addition, nano-scale rectangular pits are distributed uniformly across the surface, making a hierarchical structure. Inter-connecting edges around pits are various dimensions; the estimated size is between 6–8 µm (6.7 µm, Figure 5a, right). A binary structure of micro/nano-scale pits is therefore fabricated on Al surface by etching thus enlarging the real surface area and producing a nano-structured roughness.

After longer etching times—approximately 20 and 30 min—the number of pits increased and the size of the micro-scale pits extended due to the connection of small pits to larger holes (Figure 5b,c, left). At higher magnification (Figure 5b,c, right), the reduced size of the interconnected edges of the nano-hierarchical structure can be observed, for example, to 5.7 µm and 2.4 µm.

Such a well-controlled etching process was then further employed to fabricate a superhydrophobic surface on metal during grafting in ethanol solution of FAS-10.

3.2. Surface Wettability

The surface wettability of ground, etched and FAS-10-grafted aluminium samples was studied using water, diiodomethane and hexane (Figure 6).

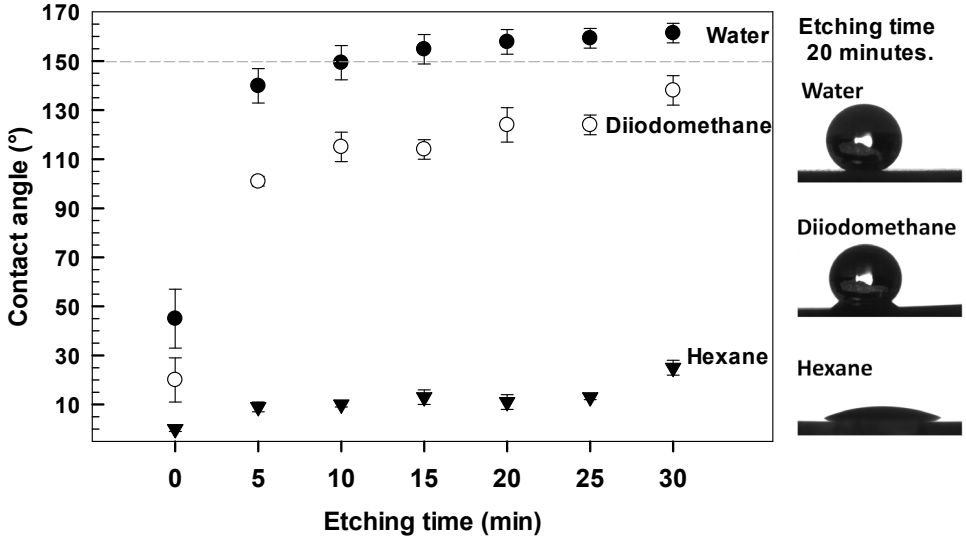

Figure 6. Contact angles measured for water, diiodomethane and hexane at aluminium surface etched for various times in 1 M $FeCl_3$ and grafted for 30 min in 1 wt.% ethanol FAS-10 solutions. The results are presented as mean values ± standard deviations. The dashed line presents the boundary of superhydrophobicity. The images of water, diiodomethane and hexane droplets on aluminium etched for 20 min and grafted with a FAS-10 are presented.

The non-ground aluminium surface was hydrophilic with a water contact angle (WCA) of about 69° due to the presence of a native oxidised layer which spontaneously forms during long exposure to air or moisture. The wettability of Al was enlarged by grinding and etching to produce a rough hydroxylated surface in $FeCl_3$-containing solution. Etched aluminium is superhydrophilic with a WCA of few degrees due to the presence of Al–OH groups formed during the etching process.

The transition from a (super)hydrophilic surface (i.e., the $FeCl_3$-etched aluminium substrate) to a (super)hydrophobic surface occurred after grafting in FAS-10 solution. It is noteworthy that the grafting of as-received or ground aluminium substrate without etching was less efficient. The water contact angle increased only up to 45°. This confirms that surface etching is crucial to fabricate a superhydrophobic surface.

The static water contact angles increase significantly with the etching time (Figure 6), in accordance with previous reports [22]. The two effects were interconnected: an increase in micro/nano roughness by prolonged etching and the presence of low surface energy molecules (FAS). After 5 min etching, the WCA was 142°, and after 20 min etching, all measured water contact angles were above 150°. If the surface was slightly tilted (less than 10°), water drops would slide from the surface confirming that the treated aluminium had a low sliding angle. Further etching does not contribute to an additional WCA increase.

The static contact angles were also measured with less polar solvents: diiodomethane and hexane (Figure 6). The CAs for diiodomethane increased with etching time, but the maximum values were below 138°. Even smaller CAs were obtained for hexane, where a maximum of 25° was reached.

From the obtained wettability data, it can be concluded that etching the surface for 20 min and grafting for 30 min in FAS-10 solution were optimal conditions to obtain superhydrophobic properties with high water repellence. Therefore, further characterisation was carried out on samples fabricated using these optimal parameters.

3.3. Composition, Topography and Morphology of Aluminium Grafted with FAS-10

3.3.1. SEM/EDS Characterisation

The organic film formed by grafting was presumably nanometre-sized and thus cannot be easily analysed by contact profilometry or by the change in sample weight. Therefore, the surface morphology of the etched and FAS-10-grafted surface was investigated by SEM/EDS. Figure 7 shows the typical morphology of aluminium etched for 20 min in $FeCl_3$ and grafted for 30 min using FAS-10.

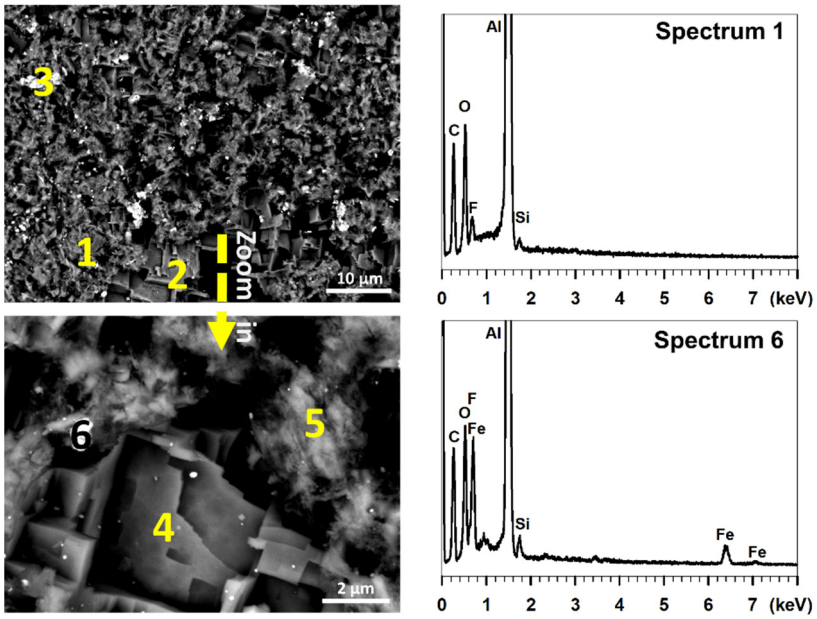

Figure 7. SEM images recorded in COMPO mode of the aluminium surface etched for 20 min in 1 M $FeCl_3$ followed by grafting for 30 min in 1 wt.% ethanol FAS-10 solution. The enumerated positions (from 1 to 6) indicate spots where the EDS analyses were performed (values are given in Table 2). Spectra 1 and 6 are shown as representatives.

Table 2. Composition determined by EDS analysis in at.% at enumerated spots on aluminium treated with FAS-10 as denoted in Figure 7.

Numbered Spots	Al	O	Fe	Si	F
1	81.6	15.2		0.5	2.7
2	61.6	24.6	5.7	1.1	7.0
3	47.6	13.8	33.7	1.4	3.5
4	98.5	1.5			
5	60.6	29.3		3.8	6.3
6	63.6	18.5	12.2	1.1	4.6

After grafting, a film of FAS-10 molecules was formed on the rough surface. Although the formed film was not observed on SEM image recorded in COMPO mode, its presence was confirmed by comparing the chemical compositions of the etched only and superhydrophobic surface using the EDS (Figure 7, Table 2).

Si and F originating from FAS-10 were detected on many analysed spots on the aluminium matrix (Figure 7, spots 1–3, spectrum 1) confirming the efficient grafting process during immersion. At higher magnification in the micro/nano-structured region (Figure 7), it can be noted that the film did not evenly cover the surface. For example, at spot 4, Si and F were not detected. It seems that Si and F were detected only at some spots on aluminium matrix (Figure 7, Spot 5, Table 2) and at spots with higher

amounts of Fe (Figure 7, spots 2, 3, 6, Table 2), indicating that these were spots with more preferable bonding due to the presence of Fe-oxide as is shown below.

3.3.2. XPS Characterisation

The XPS analysis was performed to evaluate the chemical composition of aluminium etched for 20 min in $FeCl_3$ and aluminium grafted for 30 min with FAS-10. The survey XPS spectrum of etched aluminium is presented in Appendix A Figure A1a, where the identified elements originated from the substrate (Al), the presence of passive film (Al and O), other impurities present in the aluminium (Fe) or remaining after etching (Fe and Cl) and the effect of the atmosphere (adventitious C). The chemical composition is given in Table 3.

Table 3. Composition determined by XPS analysis in at.% for aluminium surface etched for 20 min in 1 M $FeCl_3$ and aluminium grafted for 30 min in 1 wt.% ethanol FAS-10 solution (Appendix A Figure A1).

Sample	O	C	Al	Cl	Fe	F	Si
Etched aluminium surface	47.5	34.8	13.7	2.8	1.2	-	-
Grafted aluminium surface with FAS-10	26.7	26.8	7.8	-	0.5	36.8	1.4

The etched surface mainly consisted of O and Al and a small amount of Cl and Fe which is in agreement with Equation (1) and proves that Fe was predominantly precipitated into solution, leaving only a residual amount at the surface, probably presented as $FeCl_3$.

The survey XPS spectrum of the grafted aluminium with FAS-10 strongly differed from the etched aluminium, Appendix A Figure A1b. The presence of Al, Si, F, C, O and Fe confirmed the grafting of FAS-10 film on the surface. The F, C and O now became the most abundant elements (Table 3). The Al concentration decreased after grafting but was still visible, indicating that the grafting layer was thinner than 10 nm.

The etched and grafted aluminium surfaces were additionally analysed with high-energy resolution XPS spectra (Figure 8).

The Al 2p and O 1s spectra of etched aluminium confirmed the presence of aluminium oxide/hydroxide (Figure 8a,b). According to the XPS database [40–42], spectra related the presence of AlOOH (74.7 eV, 531.7 eV) and passivation during exposure to air Al_2O_3 (73.1 eV, 530.7 eV). The peak related to Fe $2p_{3/2}$ centred at 711 eV has a lot of noise due to the low intensity, confirming the presence of small amount of mixed Fe(II) oxide (multiple splitting at 709.8 eV and 711 eV [43]) and Fe(III) oxide (at 710.9 eV and 712.7 eV [43]) at the surface, Figure 8c. Moreover, XPS spectra confirm that zero-valent iron formed during etching was not present on the surface (usually detected as a peak at 706.8 eV [42–44]). The carbon presented as adventitious carbon at a single sharp peak at 284.8 eV (Figure 8d).

On the other hand, the grafted aluminium showed the broadening of the peaks for Al 2p and O 1s which reflected the presence of the third component related to Al–O–Si (at 75.5 eV and 532.7 eV, respectively) formed during the grafting in the FAS-10 solution. On the other hand, the peak for Fe $2p_{3/2}$ exhibited a similar shape to a non-grafted sample. Therefore, the XPS data confirmed the formation of the covalent bond between aluminium oxide/hydroxide and$(CH_3CH_2O)_3$–Si–$(CH_2)_2(CF_2)_7CF_3$ presented by Equation (2). This is further corroborated by the C 1s spectrum (Figure 8d). The peak can be resolved into seven components, namely, –CF_3 (294.0 eV),–CF_2 (291.8 eV), –CF-CF_x (290.8 eV), C–F (289.8 eV), –C–CF_x (286.7 eV), –C–C (284.8 eV) and –C–Si (283.8 eV). The characteristic bands of the fluoroalkyl groups (CF_2 and CF_3) confirmed the presence of FAS-10 molecules at the surface. The intensity of the CF_2 peak is equal to C–C and higher than the CF_3 peak, because the FAS-10 contains more CF_2 groups than the CF_3 and C–C bonds. The Si 2p peaks comprised three components (Figure 8e) with a bending energy at about 101.3 eV for Si–O–C, 102.5 eV for Si–C associated to FAS molecule [40,41] and at 103.7 eV associated with the Si–O–Al species formed during grafting [40,41].

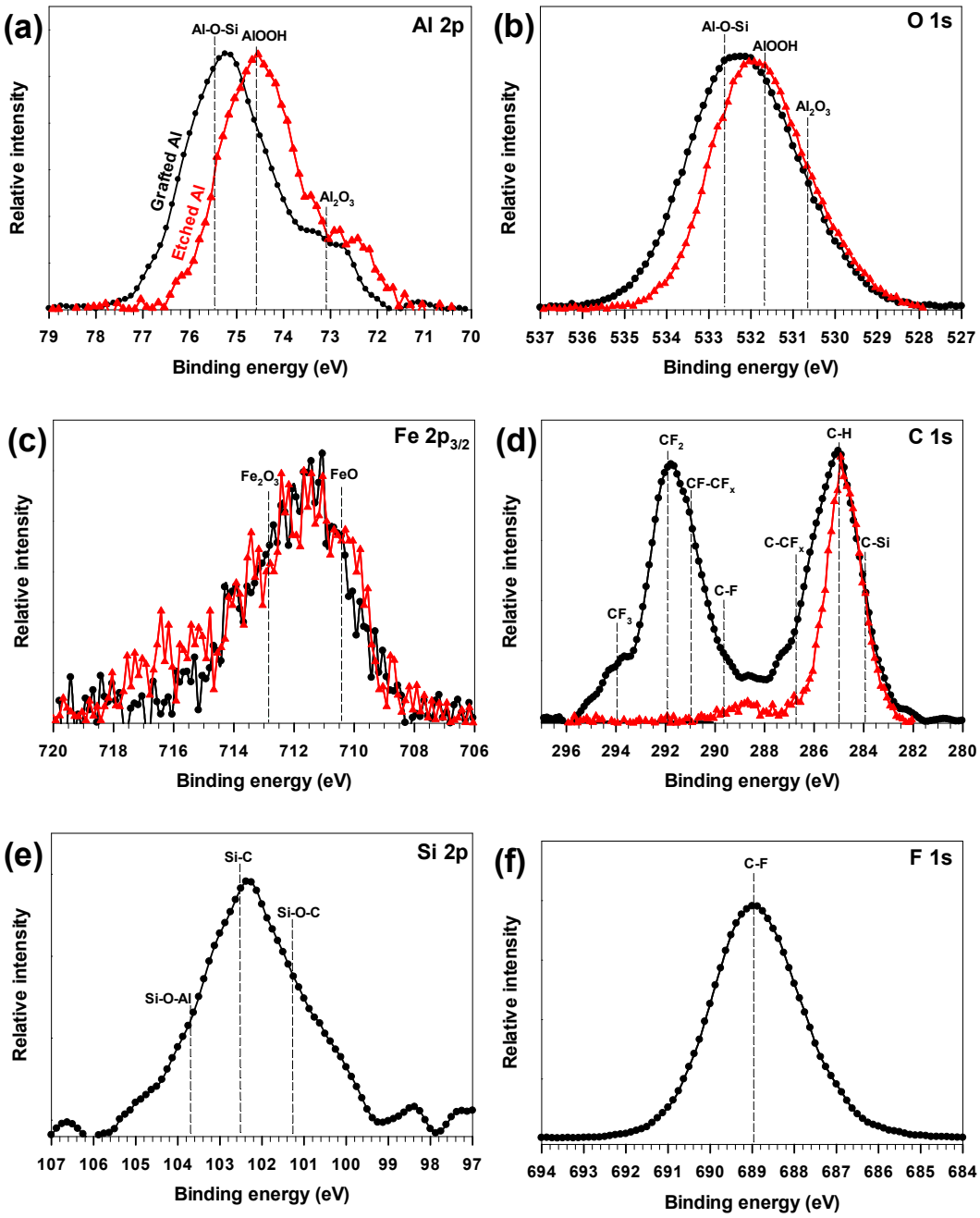

Figure 8. High-energy resolution XPS: (**a**) Al 2p, (**b**) O 1s, (**c**) Fe $2p_{3/2}$, (**d**) C 1s, (**e**) Si 2p, and (**f**) F 1s. Symbols present experimental spectra, and vertical lines present the position of component peaks. Spectra were recorded for Al etched for 20 min in 1 M $FeCl_3$ (red triangles) and grafted for 30 min in 1 wt.% ethanol FAS-10 solution (black dots).

The presence of the FAS-10 molecule can also be confirmed in F 1s spectra, where a broad peak between 686–691 eV is related to C–F covalent bond in the FAS-10 molecule (Figure 8f). The CF_3 and CF_2 concentrations present in the C 1s spectrum of the FAS-10-treated Al is in correlation with the molecular structure. The high concentration of CF_3 and CF_2 on the surface indicates that the molecules were orientated with the Si–O bond to the surface forming Si–O–Al, while the $(CH_2)_2(CF_2)_7CF_3$ tail comprised the outermost surface film. Such a surface composition is in correlation with the obtained reduced wettability.

3.4. Bounce Dynamics

The dynamic behaviour of the water drops on the etched and FAS-10-grafted aluminium surface was investigated using water drop impact tests. Treated Al surfaces maintain remarkable non-wetting, superhydrophobic properties, not only in quasi-static conditions (as typically measured by sessile drop method) but also under dynamic conditions leading to rebound of the droplet after impact.

These characteristics were evaluated from the sequential images of one water droplet during the bouncing process on the superhydrophobic surface (Figure 9, Video A1).

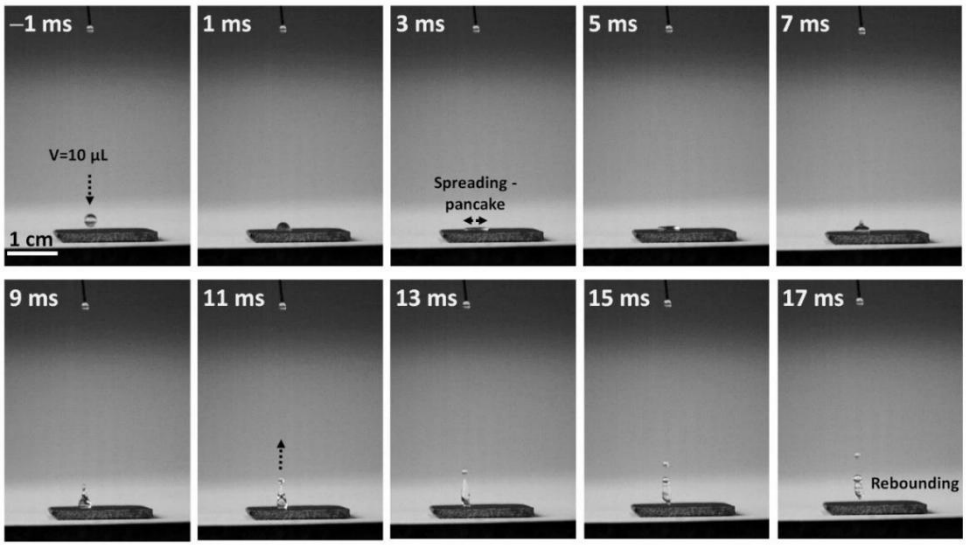

Figure 9. Time-lapsed images of a water droplet (volume 10 µL) bouncing on the horizontal aluminium surface etched for 20 min in 1 M $FeCl_3$ and followed by grafting for 30 min in 1 wt.% ethanol FAS-10 solution. Videos A1 and A2.

The process can be divided into different sequences which include falling toward the surface, impinging the surface, transforming a thin pancake and achieving a maximum contact with the surface, retracting back one water droplet followed by the formation of an inverted baseball bat which rebounds from the surface toward to a maximum height. The water droplet bounded and completely left the coated surface within 14 ms, without leaving any water residuals (Figure 9). The water droplet rebounded a few times on the superhydrophobic surface and, subsequently, left the surface or impinged on the superhydrophobic surface multiple times (Video A1).

The dynamic properties were also evaluated for a water droplet impinged to the superhydrophobic surface, which was tilted for 2° (Video A2). The water droplet rotated and rebounded and then rolled off. This experiment confirmed that even when released from a low height, a water droplet has enough kinetic energy to provide the driving force for bouncing and rotation. Consequently, the main goal to overcome low surface tension and self-gravity of a droplet to achieve the bouncing process was obtained. Moreover, the adhesion of a water droplet was efficiently reduced, and it did not remain on the superhydrophobic surface.

3.5. Self-Cleaning Ability

The self-cleaning test was carried out to demonstrate the removal of solid pollutants (featured by carbon nanotube particles as pollutants) from the treated aluminium surface (Figure 10, Video A3). Pollutants remained on the untreated (ground) aluminium surface which was wetted and contaminated by the particles dispersed in water (Figure 10).

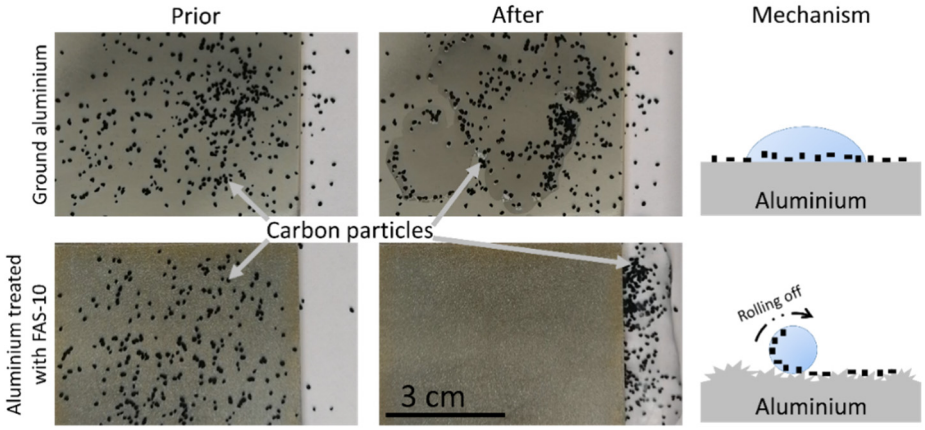

Figure 10. The appearance of ground and treated aluminium surfaces (etched for 20 min in 1 M $FeCl_3$ and followed by grafting for 30 min in 1 wt.% ethanol FAS-10 solution) covered with carbon particles prior and after rinsing with tap water. Video A3. The proposed mechanism of self-cleaning on ground and treated surfaces is presented schematically.

The mechanism is presented schematically in Figure 10. This behaviour indicates that ground aluminium does not have a self-cleaning ability. In contrast, no pollutants or water droplets remained on aluminium treated in FAS-10, because water removes the dirt when water droplets roll (Figure 10, Video A3). This illustrates its excellent water-repelling and self-cleaning ability, as the superhydrophobic aluminium surface does not allow water droplets to penetrate into the grooves, but rather they are suspended on the micro/nano-scale pits. Water droplets cannot stick to the surface and depart easily without a distinct distortion. Low adhesion of the superhydrophobic surface allows droplets to roll off quite easily and get rid of various external contaminants, just like the natural lotus leaf, according to the mechanism schematically presented in Figure 10. This behaviour has been theoretically explained by the Cassie and Baxter equation [5,28,37].

The superhydrophobicity of etched and FAS-10-grafted surfaces results from a hierarchically rough surface covered by an organic film whose low surface energy allows the air to be trapped in "pockets" areas between the water droplets and solid surface thus minimising their contact.

3.6. Anti-Icing Ability

The anti-icing properties of the superhydrophobic surface were characterised using conditions simulating the real environment. To evaluate this effect, two critical aspects have to be considered: icing-delay performance and ice adhesion strength. The icing-delay performance of water droplets deposited on the treated aluminium surface was evaluated in a reverse direction as completely melting delay (i.e., melting-delay time). Figure 11a (Video A4) shows the melting processes of droplets on the treated surfaces frozen at −15 °C. The droplet on the ground surface was quickly melted (120 s); in contrast, the droplets on the treated aluminium surface took longer (260 s) to melt.

The melting process was additionally characterised using the thermal infrared camera (Figure 11b). The droplets on the ground aluminium surface started to melt after 60 s near the edges, some were melted and after 90 s, ice remained only in the centre of larger droplets. Ice was completely melted after 120 s. Frozen droplets on treated aluminium melted much slower (Figure 11a,b, Video A4). After 60 s, the droplets remained frozen, and slow melting can be seen after 120 s up to 260 s.

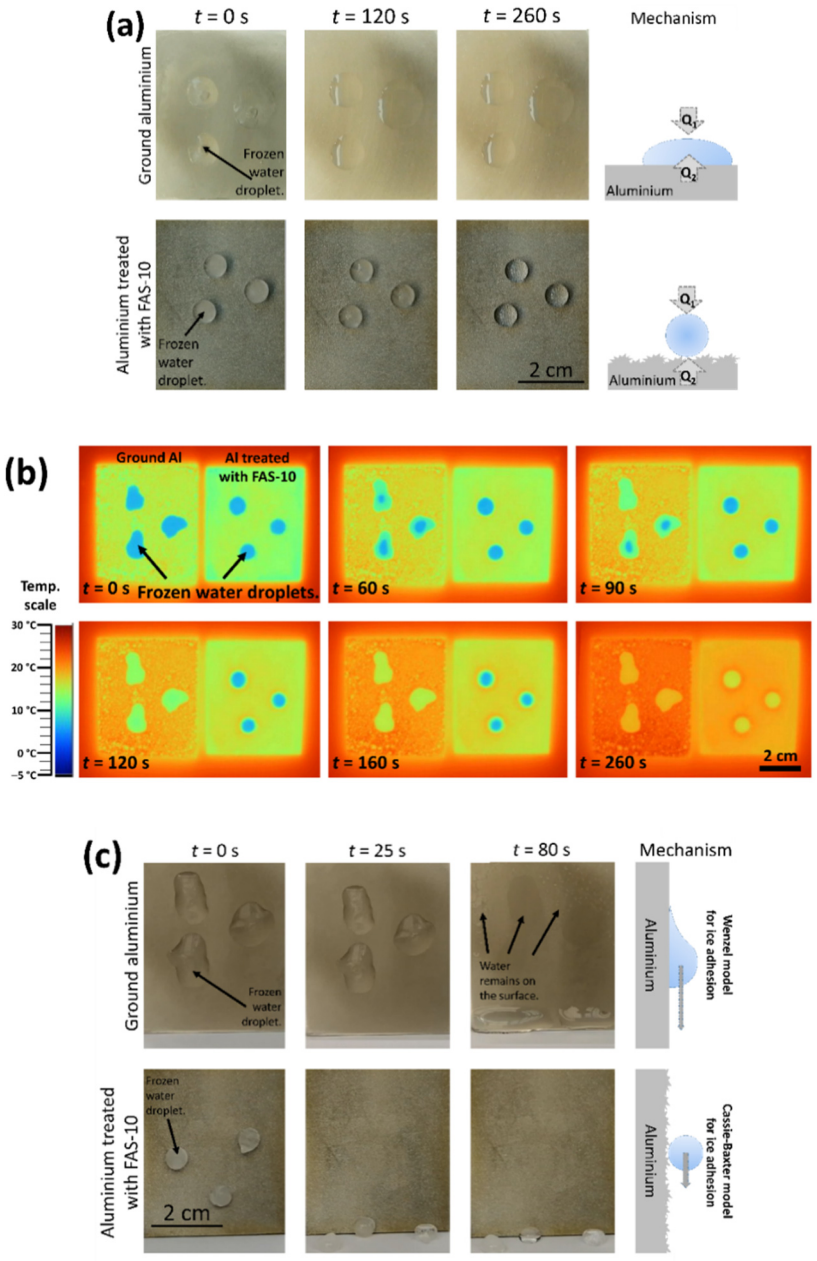

Figure 11. Frames of the de-icing process on ground and treated surfaces after various times (positioned horizontally) after taking the samples from the freezer (−15 °C) to ambient temperature followed using a (**a**) digital camera and (**b**) thermal infrared camera. Figure (**c**) shows the effect on the ice adhesion on the ground and treated aluminium (positioned vertically). Videos A4 and A5. The proposed mechanism of melting-delay and adhesion on ground and treated surfaces are presented schematically in (**a**) and (**c**).

This melting delay is in accordance with thermodynamics. The droplet on the cold surface gains heat from the air in the forms of heat conduction and thermal radiation and absorbs heat by heat conduction, schematically presented in Figure 11a. The difference in the temperature can be expressed according to the absorbed energy of droplet as per Equation (3) [45]:

$$\Delta T = \frac{\rho c_p (T_0 - T_1)}{Q_1 - Q_2} = \frac{\rho c_p (T_0 - T_1)}{\Delta Q} \quad (3)$$

where ΔT is the increased temperature of the droplet; ρ is the water density; c_p is the specific heat capacity of the water; T_0 is the starting temperature of the droplet; T_1 is the sample surface temperature; ΔQ is the net heat increase in unit time; Q_1 is the heat gain from the air; and Q_2 is the heat absorbed from contact with a solid surface. A small Q_2 or a large Q_1 can cause a large ΔQ and results in a small ΔT. Thus, it can explain why droplets suspended on superhydrophobic surfaces (treated aluminium) have a longer melting delay time compared to ground surfaces.

A difference in the heating of the surface area where the droplets were not present was also observed (Figure 11a,b). On the surface of the ground sample, there were small droplets of the water, confirming that the water condensed on the surface during melting. The treated surface was heated more evenly and no water condensed on the surface due to the trapped air in the structure pockets which acts as a thermal insulator.

Figure 11c shows the adhesion of the frozen droplet on the ground and treated aluminium surfaces (Video A5). According to the Wenzle wetting model of the droplet on the aluminium surface, the ice adhesion strength is related to the contact area fractions (f_1) of the liquid droplet on the solid. In the Cassie–Baxter model of the superhydrophobic surface, the actual contact interface is between ice and ice/air pockets and ice/hydrophobic solid, leading to a lower ice adhesion strength. Both mechanisms are presented schematically in Figure 11c. The breakage of the contact between formed ice and superhydrophobic surface practically occurs only along with the real contact interface between ice and solid. Consequently, the measured ice adhesion strength on the superhydrophobic surface is much smaller compared to hydrophilic or hydrophobic aluminium.

The anti-icing properties were additionally tested when placing the ground and treated aluminium samples in the freezer (T = −15 °C) and dropping the cold water onto the surface (Figure 12). The obtained results vividly demonstrate that, on the ground surface, the water droplets were spread on the surface, began to freeze immediately and formed ice film on the entire surface (Figure 12a). In contrast, on the treated aluminium, no film was observed because the droplets bounced or rolled off the surface (Figure 12b); therefore, the aluminium surface remained unsaturated with water despite a continuous water drip.

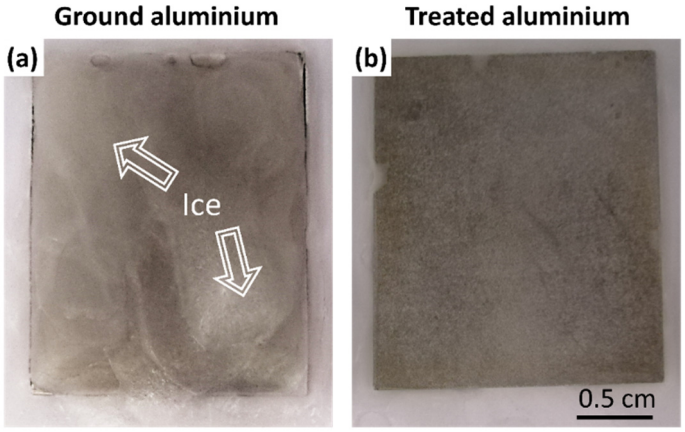

Figure 12. (**a**) The icing process for ground aluminium and (**b**) treated aluminium during testing in the freezer at −15 °C while dropping cold water droplets on the surface for 5 min.

The results confirm that the superhydrophobic aluminium exhibited a high anti-icing potential with the icing-delay and lower ice adhesion and ice film formation on the treated aluminium surface.

4. Conclusions

A (super)hydrophobic aluminium surface was fabricated using a simple, low-cost, two-step process consisting of chemical etching in $FeCl_3$ solution followed by grafting using perfluoroalkyl silane (FAS-10).

The topography and the weight loss of the surface confirm that $FeCl_3$ strongly promotes etching of Al; the effect is time-dependent. Roughening of the aluminium surface by etching in the $FeCl_3$ solution was found to be a crucial parameter to provide a micro/nano-pattern and aluminium oxide/hydroxide structure which then acts as an active surface for further grafting with perfluoroalkyl silane film.

An optimal etching time of 20 min and grafting for 30 min in FAS-10 solution resulted in superhydrophobic aluminium surface with a water contact angle above 150° and a low sliding angle below < 10°.

The XPS data confirmed that the FAS molecules were covalently bonded on the aluminium surface.

The superhydrophobic aluminium surface showed excellent dynamic properties, seen as a bouncing effect without leaving any residual water on the surface. Consequently, such a treated surface showed an excellent self-cleaning ability. Low contact of a water droplet with the treated surface also affected the melting delay, indicating an improved anti-icing effect.

This fabricated aluminium surface is a great candidate for various applications because of the properties gained to increase the durability and functionality of aluminium during exposure to the real environment.

Author Contributions: P.R. prepared the specimens, performed the weight loss, contact angle and profilometer measurements, and evaluated the self-cleaning and anti-icing abilities. The co-authors contributed to the evaluation and discussion on the following techniques employed in this study: B.K., the SEM/EDS results; M.P., the results obtained by the ultra-high-speed camera; I.M., the XPS results. Moreover, P.R. and I.M. wrote the majority of the paper. All authors have read and agreed to the published version of the manuscript.

Funding: This work is a part of M-ERA.NET project entitled "Design of Corrosion Resistant Coatings Targeted for Versatile Applications" (acronym COR_ID). The financial support from the Slovenian Research Agency (research core funding No. P2-0393 and P1-0134) is also acknowledged.

Acknowledgments: The authors thank Primož Fajdiga and Simon Iskra for their valuable technical help.

Conflicts of Interest: The authors declare no conflict of interest.

Appendix A

The following figure of XPS survey spectra complements the high-energy resolution spectra presented in Figure 8.

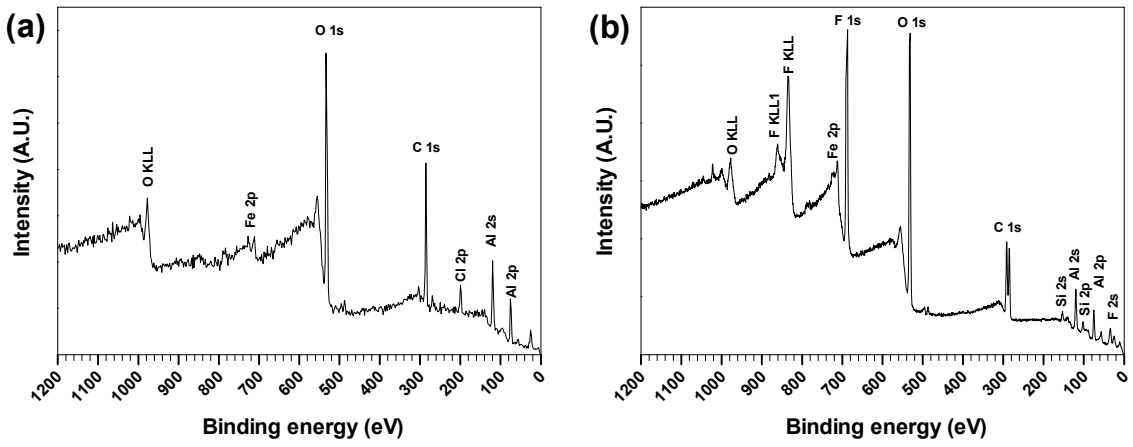

Figure A1. Survey XPS spectra recorded for (**a**) aluminium surface etched for 20 min in 1 M $FeCl_3$ and (**b**) grafted for 30 min in 1 wt.% ethanol FAS-10 solution.

Appendix B

The following videos complement the data and Figures 9–11 in this article. They are available in the online version.

Video A1. Bouncing dynamic characterisation

Video A2. Water rolling off the surface

Video A3. Self-cleaning of solid pollutants
Video A4. Anti-icing properties and melting delay
Video A5. Ice adhesion on ground and treated aluminium

References

1. Hatch, J.E. *Aluminum: Properties and Physical Metallurgy*; ASM International: Cleveland, OH, USA, 1984; ISBN 13 9780871701763.
2. Zhang, D.; Wang, L.; Qian, H.; Li, X. Superhydrophobic surfaces for corrosion protection: a review of recent progresses and future directions. *J. Coat. Technol. Res.* **2016**, *13*, 11–29. [CrossRef]
3. Vazirinasab, E.; Jafari, R.; Momen, G. Application of superhydrophobic coatings as a corrosion barrier: A review. *Surf. Coat. Technol.* **2018**, *341*, 40–56. [CrossRef]
4. Latthe, S.S.; Gurav, A.B.; Maruti, C.S.; Vhatkar, R.S. Recent Progress in Preparation of Superhydrophobic Surfaces: A Review. *J. Surf. Eng. Mater. Adv. Technol.* **2012**, *02*, 76–94.
5. Shirtcliffe, N.J.; McHale, G.; Atherton, S.; Newton, M.I. An introduction to superhydrophobicity. *Adv. Colloid Interface* **2010**, *161*, 124–138. [CrossRef] [PubMed]
6. Barati Darband, G.; Aliofkhazraei, M.; Khorsand, S.; Sokhanvar, S.; Kaboli, A. Science and Engineering of Superhydrophobic Surfaces: Review of Corrosion Resistance, Chemical and Mechanical Stability. *Arab. J. Chem.* **2020**, *13*, 1763–1802. [CrossRef]
7. Mohamed, A.M.A.; Abdullah, A.M.; Younan, N.A. Corrosion behavior of superhydrophobic surfaces: A review. *Arab. J. Chem.* **2015**, *8*, 749–765. [CrossRef]
8. Rodič, P.; Milošev, I. One-step ultrasound fabrication of corrosion resistant, self-cleaning and anti-icing coatings on aluminium. *Surf. Coat. Technol.* **2019**, *369*, 175–185. [CrossRef]
9. Milošev, I.; Bakarič, T.; Zanna, S.; Seyeux, A.; Rodič, P.; Poberžnik, M.; Chiter, F.; Cornette, P.; Costa, D.; Kokalj, A.; et al. Electrochemical, Surface-Analytical, and Computational DFT Study of Alkaline Etched Aluminum Modified by Carboxylic Acids for Corrosion Protection and Hydrophobicity. *J. Electrochem. Soc.* **2019**, *166*, C3131–C3146. [CrossRef]
10. Cao, L.; Jones, A.K.; Sikka, V.K.; Wu, J.; Gao, D. Anti-Icing Superhydrophobic Coatings. *Langmuir* **2009**, *25*, 12444–12448. [CrossRef]
11. Kreder, M.J.; Alvarenga, J.; Kim, P.; Aizenberg, J. Design of anti-icing surfaces: smooth, textured or slippery? *Nat. Rev. Mater.* **2016**, *1*, 1–15. [CrossRef]
12. Wang, L.; Gong, Q.; Zhan, S.; Jiang, L.; Zheng, Y. Robust Anti-Icing Performance of a Flexible Superhydrophobic Surface. *Adv. Mater.* **2016**, *28*, 7729–7735. [CrossRef] [PubMed]
13. Nurioglu, A.G.; Esteves, A.C.C.; With, G. de Non-toxic, non-biocide-release antifouling coatings based on molecular structure design for marine applications. *J. Mater. Chem. B* **2015**, *3*, 6547–6570. [CrossRef]
14. Hizal, F.; Rungraeng, N.; Lee, J.; Jun, S.; Busscher, H.J.; van der Mei, H.C.; Choi, C.-H. Nanoengineered Superhydrophobic Surfaces of Aluminum with Extremely Low Bacterial Adhesivity. *ACS Appl. Mater. Interfaces* **2017**, *9*, 12118–12129. [CrossRef] [PubMed]
15. Lakshmi, R.V.; Bharathidasan, T.; Basu, B.J. Superhydrophobic sol-gel nanocomposite coatings with enhanced hardness. *Appl. Surf. Sci.* **2011**, *257*, 10421–10426. [CrossRef]
16. Zhang, Y.; Wu, J.; Yu, X.; Wu, H. Low-cost one-step fabrication of superhydrophobic surface on Al alloy. *Appl. Surf. Sci.* **2011**, *257*, 7928–7931. [CrossRef]
17. Zhang, B.; Zhu, Q.; Li, Y.; Hou, B. Facile fluorine-free one step fabrication of superhydrophobic aluminum surface towards self-cleaning and marine anticorrosion. *Chem. Eng. J.* **2018**, *352*, 625–633. [CrossRef]
18. Biloiu, C.; Biloiu, I.A.; Sakai, Y.; Suda, Y.; Ohta, A. Amorphous fluorocarbon polymer (a-C:F) films obtained by plasma enhanced chemical vapor deposition from perfluoro-octane (C8F18) vapor I: Deposition, morphology, structural and chemical properties. *J. Vac. Sci. Technol. A* **2003**, *22*, 13–19. [CrossRef]
19. Huang, Y.; Sarkar, D.K.; Grant Chen, X. Superhydrophobic aluminum alloy surfaces prepared by chemical etching process and their corrosion resistance properties. *Appl. Surf. Sci.* **2015**, *356*, 1012–1024. [CrossRef]
20. Varshney, P.; Mohapatra, S.S.; Kumar, A. Superhydrophobic coatings for aluminium surfaces synthesized by chemical etching process. *Int. J. Smart Nano Mater.* **2016**, *7*, 248–264. [CrossRef]
21. Çakır, O. Chemical etching of aluminium. *J. Mater. Process. Technol.* **2008**, *199*, 337–340. [CrossRef]

22. Tong, W.; Xiong, D.; Wang, N.; Yan, C.; Tian, T. Green and timesaving fabrication of a superhydrophobic surface and its application to anti-icing, self-cleaning and oil-water separation. *Surf. Coat. Technol.* **2018**, *352*, 609–618. [CrossRef]
23. Vander Voort, G.F. *Metallography: Principles and Practice*, 6th ed.; ASM International: New York, NY, USA, 1984; ISBN 978-0-87170-672-0.
24. Qian, B.; Shen, Z. Fabrication of Superhydrophobic Surfaces by Dislocation-Selective Chemical Etching on Aluminum, Copper, and Zinc Substrates. *Langmuir* **2005**, *21*, 9007–9009. [CrossRef] [PubMed]
25. Kim, J.-H.; Mirzaei, A.; Kim, H.W.; Kim, S.S. Realization of superhydrophobic aluminum surfaces with novel micro-terrace nano-leaf hierarchical structure. *Appl. Surf. Sci.* **2018**, *451*, 207–217. [CrossRef]
26. Liu, L.; Feng, X.; Guo, M. Eco-Friendly Fabrication of Superhydrophobic Bayerite Array on Al Foil via an Etching and Growth Process. *J. Phys. Chem. C* **2013**, *117*, 25519–25525. [CrossRef]
27. Patil, D.H.; Thorat, S.B.; Khake, R.A.; Mudigonda, S. Comparative Study of $FeCl_3$ and $CuCl_2$ on Geometrical Features Using Photochemical Machining of Monel 400. *Procedia CIRP* **2018**, *68*, 144–149. [CrossRef]
28. Zhan, Z.; Li, Z.; Yu, Z.; Singh, S.; Guo, C. Superhydrophobic Al Surfaces with Properties of Anticorrosion and Reparability. *ACS Omega* **2018**, *3*, 17425–17429. [CrossRef]
29. Parin, R.; Col, D.D.; Bortolin, S.; Martucci, A. Dropwise condensation over superhydrophobic aluminium surfaces. *J. Phys. Conf. Ser.* **2016**, *745*, 1–8. [CrossRef]
30. Ruan, M.; Li, W.; Wang, B.; Deng, B.; Ma, F.; Yu, Z. Preparation and anti-icing behavior of superhydrophobic surfaces on aluminum alloy substrates. *Langmuir* **2013**, *29*, 8482–8491. [CrossRef]
31. Nishino, T.; Meguro, M.; Nakamae, K.; Matsushita, M.; Ueda, Y. The Lowest Surface Free Energy Based on $-CF_3$ Alignment. *Langmuir* **1999**, *15*, 4321–4323. [CrossRef]
32. Bernagozzi, I.; Antonini, C.; Villa, F.; Marengo, M. Fabricating superhydrophobic aluminum: An optimized one-step wet synthesis using fluoroalkyl silane. *Colloids Surf, A Physicochem Eng Asp.* **2014**, *441*, 919–924. [CrossRef]
33. Brassard, J.-D.; Sarkar, D.K.; Perron, J. Fluorine Based Superhydrophobic Coatings. *Appl. Sci.* **2012**, *2*, 453–464. [CrossRef]
34. Saleema, N.; Sarkar, D.K.; Gallant, D.; Paynter, R.W.; Chen, X.-G. Chemical Nature of Superhydrophobic Aluminum Alloy Surfaces Produced via a One-Step Process Using Fluoroalkyl-Silane in a Base Medium. *ACS Appl. Mater. Interfaces* **2011**, *3*, 4775–4781. [CrossRef] [PubMed]
35. Poberžnik, M.; Costa, D.; Hemeryck, A.; Kokalj, A. Insight into the Bonding of Silanols to Oxidized Aluminum Surfaces. *J. Phys. Chem. C* **2018**, *122*, 9417–9431. [CrossRef]
36. Poberžnik, M.; Kokalj, A. Implausibility of bidentate bonding of the silanol headgroup to oxidized aluminum surfaces. *Appl. Surf. Sci.* **2019**, *492*, 909–918. [CrossRef]
37. Kumar, A.; Gogoi, B. Development of durable self-cleaning superhydrophobic coatings for aluminium surfaces via chemical etching method. *Tribol. Int.* **2018**, *122*, 114–118. [CrossRef]
38. Rao, P.N.; Kunzru, D. Fabrication of microchannels on stainless steel by wet chemical etching. *J. Micromech. Microeng.* **2007**, *17*, N99–N106.
39. Poberžnik, M. Quantum mechanical modeling of the oxidation of aluminum surfaces and their interactions with corrosion inhibitors. Ph.D. Thesis, University of Ljubljana, Ljubljana, Slovenia, 2019; pp. 75–83.
40. Milošev, I.; Jovanović, Ž.; Bajat, J.B.; Jančić-Heinemann, R.; Mišković-Stanković, V.B. Surface Analysis and Electrochemical Behavior of Aluminum Pretreated by Vinyltriethoxysilane Films in Mild NaCl Solution. *J. Electrochem. Soc.* **2012**, *159*, C303–C311. [CrossRef]
41. Bajat, J.B.; Milošev, I.; Jovanović, Ž.; Jančić-Heinemann, R.M.; Dimitrijević, M.; Mišković-Stanković, V.B. Corrosion protection of aluminium pretreated by vinyltriethoxysilane in sodium chloride solution. *Corros. Sci.* **2010**, *52*, 1060–1069. [CrossRef]
42. NIST X-ray Photoelectron Spectroscopy Database. *NIST Standard Reference Database Number 20*; National Institute of Standards and Technology: Gaithersburg, MD, USA, 2000; Volume 2000. [CrossRef]
43. Milošev, I.; Strehblow, H.-H. The behavior of stainless steels in physiological solution containing complexing agent studied by X-ray photoelectron spectroscopy. *J. Biomed. Mater. Res.* **2000**, *52*, 404–412. [CrossRef]

44. Santana, I.; Pepe, A.; Jimenez-Pique, E.; Pellice, S.; Milošev, I.; Ceré, S. Corrosion protection of carbon steel by silica-based hybrid coatings containing cerium salts: Effect of silica nanoparticle content. *Surf. Coat. Tech.* **2015**, *265*, 106–116. [CrossRef]
45. Shen, Y.; Tao, J.; Tao, H.; Chen, S.; Pan, L.; Wang, T. Superhydrophobic Ti_6Al_4V surfaces with regular array patterns for anti-icing applications. *RSC Adv.* **2015**, *5*, 32813–32818. [CrossRef]